Reduced Rating Active Phase Converter for Three-Phase Induction Generator Based Single Phase Grid-Tied Systems

Anil K Adapa and Vinod John, *Senior Member, IEEE*

***Abstract*—The distribution systems and microgrids in remote, and rural areas are often of a single-phase nature due to economic viability. Fixed frequency three-phase induction generators (IGs) are popular in such applications due to their competitive performance features, and utility. This article proposes a control approach for injecting power to a single-phase grid from an active phase converter (APC) assisted three-phase IG. The presented approach ensures a balanced operation of the IG even with variable generation. This work proposes a method of using an ac auxiliary capacitor that reduces the APC pole currents and improves the converter efficiency. Closed-form expression of the grid current and converter pole currents for a given operating point of the IG are derived. Based on the analysis, and the converter current expressions, a procedure to find the optimal auxiliary capacitance for a given operating point of the IG is presented. Experimental results are provided to validate the theoretical framework, and APC control approach. The experimental results demonstrate the injection of 2.4 kW real power into the single-phase grid at near unity factor and validate the proposed control of the APC-IG system.**

***Index Terms*—Active phase-converter (APC), auxiliary capacitor, converter currents, distributed generation, induction generator (IG), phasor analysis, pulsewidth modulation (PWM) converter.**

I. Introduction

THREE-PHASE supply may not be available in remote regions and rural areas, and one has to rely upon the microgrids due to inaccessible geographical conditions [1], [2]. Often the loads in such locations are single-phase in nature [3]. Supplying power to such loads with low-cost generation or co-generation systems, which access nonconventional energy sources like wind and hydropower is preferred [4]–[6]. Squirrel cage induction machine based wind, micro hydel, and distributed generation schemes are attractive solutions due to the simplicity and advantages of availability, low cost, and reduced maintenance needs [1], [4].

Operating a three-phase induction generator (IG) with a single-phase load is an extreme case of unbalance, resulting in pulsating developed torque which is detrimental to the drive train [7]. IG needs to be derated to operate within the allowable thermal limits due to the undesirable rotor current harmonics [1]. Steinmetz connection using a single excitation capacitor is a simple method to reduce the unbalanced voltages and currents in the IG system [8]. Two excitation capacitors based methods [5], [9], and transformer-based current injection technique in conjunction with excitation capacitors [4] offer reasonable phase balance and improve the power factor of the current injected into the grid. However, these passive self-excitation schemes are suitable only where the load voltage and frequency regulations are not stringent.

Three-phase grid connected IG based schemes are well established in literature [10]–[12]. These IGs are driven beyond the synchronous speed to inject power to the grid and draws necessary reactive power for the excitation from the grid. In [10], extensive studies are carried out on different aspects such as grid voltage disturbance and variations of input mechanical power, for obtaining suitable capacitors required for reactive power support. Thyristor converter based reactive power volt-ampere reactive (VAR) compensation technique on the IG is presented in [11]. Variable excitation capacitors and on-load tap changer transformer based approach to improve power transfer capability in grid connected IG systems is presented in [12]. All these techniques are not directly applicable to inject power from a three-phase IG to a single-phase connection for remote and rural areas. Converter assisted techniques for single-phase IGs in stand-alone and grid-connected applications is presented in literature [13], [14]. However, there are availability and cost limitations of single-phase IGs in the medium to high power range. These converter assisted techniques can be extended to three-phase IG, but at the cost of reducing the maximum power output of the IG that is delivered to a single-phase grid or load, as one of the windings is used to deliver power and the others are for excitation control [14].

An active phase converter (APC) aids in obtaining balanced loading of a three-phase IG powering single-phase or unbalanced load. A reduced switch APC control to inject power from a three-phase IG to a single-phase grid resulting in balanced

Manuscript received January 21, 2020; revised August 18, 2020; accepted September 9, 2020. Date of publication October 1, 2020; date of current version December 31, 2020. Paper 2019-SECSC-1578.R1, presented at the 2018 IEEE International Conference on Power Electronics, Drives and Energy Systems, Chennai, India, Dec. 18–21, and approved for publication in the IEEE TRANSACTIONS ON INDUSTRY APPLICATIONS by the Renewable and Sustainable Energy Conversion Systems Committee of the IEEE Industry Applications Society. This work was supported by the Central Power Research Institute, Ministry of Power, Government of India, under the project Power Conversion, Control, and Protection Technologies for Microgrid. *(Corresponding author: Anil K Adapa.)*

The authors are with the Department of Electrical Engineering, Indian Institute of Science, Bangalore 560012, India (e-mail: anilkumaradapa@gmail.com; vjohn@iisc.ac.in).

Color versions of one or more of the figures in this article are available online at https://ieeexplore.ieee.org.

Digital Object Identifier 10.1109/TIA.2020.3028294

loading of the IG by creating a virtual third phase is presented in [15]. There are two possible cases to generate a balanced three-phase supply using APC, where 1) the line voltage v_{cb} leads v_{ab} and (ii) the line voltage v_{cb} lags v_{ab}. In literature, it is shown that the case 1), where v_{cb} leads v_{ab} results in a significant reduction in the converter currents for IG [15]. Whereas, case 2) is preferred for inductive loads [8], [16]. An auxiliary capacitor assisted APC (AC-APC) presented in [17] shows that an additional ac capacitor in the APC circuit reduces the APC currents significantly and improves the system efficiency. Double the fundamental frequency current component in the dc-bus is also reduced with the use of an additional ac capacitor [18]. But, the work presented in [8], [16]–[18] is limited to only inductive loads such as induction motors. It is shown in this article that the methods used in [8], [16]–[18] for a motor cannot be directly extended to an IG. It is shown that the converter control needs to change to achieve the benefits claimed in [8] while operating with an IG. This work also explores the topology and value of AC that should be used in the APC circuit to gain the benefits of reduction in converter currents, similar to the work presented [17] for the induction machine (IM) loads, in the case of a three-phase IG connected to a single-phase grid. The literature shows that the reduction in APC currents is a function of the load power factor, the location of AC and the APC control or phase angle relation between the grid voltage and synthesized third line voltage by APC. For IM and IG the same phase sequence is not optimal from the perspective of real and reactive power shared by the grid and the converter [15]. The IG and IM have real power components of opposite polarities and the front end converter (FEC) current also changes sign for motor and generator loads. These changes and the asymmetry in APC currents requires a detailed analytical and experimental work to attain the benefits of AC based methods in the case of IG.

The contributions of this work are:

1) facilitating injection of real power from a three-phase IG to a single-phase grid at unity power factor (UPF) using the APC;
2) determination of phase sequence for operation of the APC and IG to have reduced current stress on the converter;
3) a phasor diagram based qualitative analysis for identifying the location of auxiliary ac capacitor to reduce the APC pole currents;
4) providing an analytical framework to obtain the rms pole currents of the APC with AC;
5) an optimal AC selection criterion;
6) experimental validation of the APC with AC for injection of power from a three-phase IG to a single-phase grid at UPF.

Section II introduces the APC topology, the ways to generate a three-phase supply, and a preferred control approach for the APC with IG. The phasor analysis is used to evaluate the effect of the AC on the APC, is presented in Section III. The derivation of APC pole currents and optimal AC selection is explained in Section IV. The experimental results are discussed in Section V, followed by conclusions in Section VI.

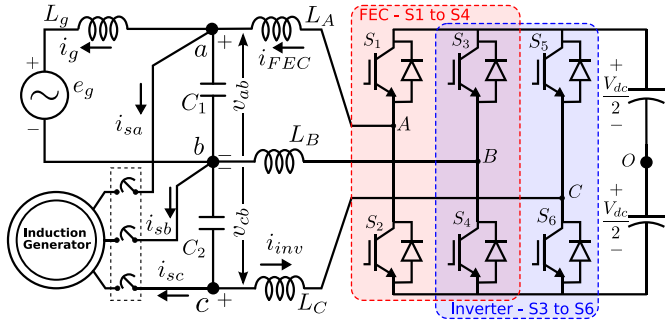

Fig. 1. APC for injecting power to single-phase connection using a three-phase IG.

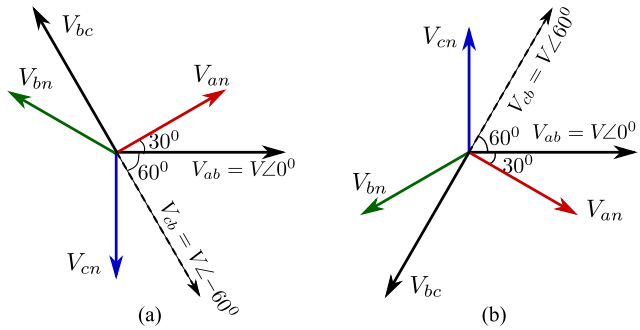

Fig. 2. Possible ways of generating three-phase voltages using APC. (a) v_{cb} lagging grid voltage, v_{ab}, preferred for IM and (b) v_{cb} leading the grid voltage, v_{ab}, preferred for IG.

II. Active Phase Converter Circuit

Fig. 1 shows an APC topology with bi-directional power processing capability [8]. Two legs of the APC, A and B establish the required dc bus voltage by operating as a single-phase FEC with an LCL filter consisting of two inductors (L) and a capacitor (C). The desired fundamental voltage v_{cb} at the output of *LC* filter is achieved by suitably controlling the converter legs B and C as a single-phase inverter. As the converter leg-B is shared between both FEC and inverter, the line voltages v_{ab} and v_{cb} are referred for analysis instead of the typical convention of the line voltage v_{ab} and v_{bc} for analysis in this work. However, the line voltage $v_{cb} = -v_{bc}$. The APC realizes balanced three-phase supply at the load terminals by controlling the magnitude of v_{cb} to be the same as that of the grid voltage at the point of common coupling (PCC), v_{ab}, with a phase shift of 60°as shown in Fig. 2. This is possible if v_{cb} lags or leads v_{ab} by 60°, as in both cases, a balanced three-phase supply is achieved. The two methods have different phase sequences. The literature [8], [17] shows that the phase sequence in Fig. 2(a) is preferred for IM. In this work, the analysis and experimental results validate that the same phase sequence can not be directly applied to IG, the phase sequence shown in Fig. 2(b) would be beneficial for IG in terms of the converter currents as explained in Section III.

In order to operate the APC in conjunction with an IG, a phasor based approach is utilized for the generation of appropriate references for the converter controller. The proposed technique

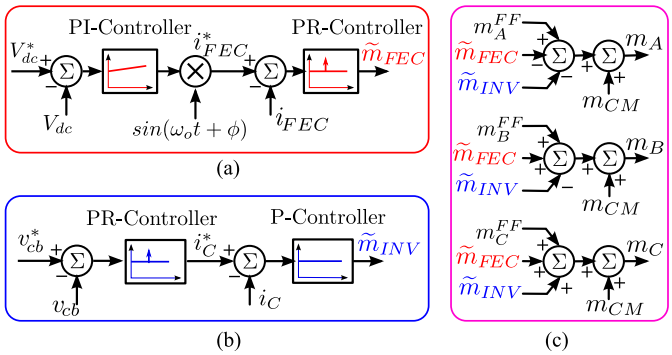

Fig. 3. Block diagram of the APC control. (a) FEC controller to maintain UPF at grid and support the dc-link voltage. (b) Inverter control to generate balanced three-phase supply. (c) Decoupling of FEC and inverter controllers with a shared leg.

has the added benefit of reduced device current stress and improved power factor at the grid.

A. Control Approach

The APC control presented in [8] and [17] uses a voltage reference generation resulting in v_{cb} that lags v_{ab} due to the inductive load that is employed. For IG operation where real power injected to the grid and inductive reactive power drawn from the grid, v_{cb} leading v_{ab} is preferred in terms of the peak current requirement of the FEC and the grid power factor [15].

The single-phase FEC of APC employs a proportional and resonant controller based inner current loop to track the reference current i^*_{FEC} as shown in Fig. 3(a). A proportional and integral controller based FEC outer voltage loop [19] maintains the APC dc-link voltage, V_{dc}, at a desired reference voltage, V^*_{dc}. The FEC with LCL mitigates the ripple current injected into the grid. The APC uses an *LC* filter at converter legs B and C, which maintains the power quality at the IG terminals by filtering the harmonic content of the PWM line voltage.

The inverter control is a cascaded two loop structure as shown in Fig. 3(b), where the outer voltage loop controller generates the current reference to the inner loop to track the sensed v_{cb} with the reference signal v^*_{cb}. A virtual resistor based active damping of inner current loop damping the *LC* resonance [20].

The decoupled control of FEC and the inverter of the APC with a shared converter Leg-B, shown in Fig. 3(c), is achieved using a similar control method presented in [8]. Three-phase IG experiences a balanced three-phase terminal voltage, by controlling the devices of converter Leg-B and Leg-C appropriately. The modulating signals, m^{FF}_A, m^{FF}_B, and m^{FF}_C are the feed-forward terms, and m_{CM} is the common-mode signal used to improve the dc-link utilization.

III. Analysis

The IG draws the required reactive power for excitation from the grid and APC. The IG delivers a part of real power directly to the grid while the remaining power is delivered to the inverter, which is in-turn injected to the grid by the FEC. The work presented in [15] shows that the control where v_{cb} leads v_{ab} for APC with IG reduces the loading on the FEC (APC leg-A current) and the reactive power demand from the grid. The qualitative analysis in this section shows that the addition of an AC reduces the APC leg-B and C currents.

A. Phasor Analysis

In this section closed-form expressions for the grid and FEC currents of the APC with the proposed control are derived. Reactive power associated with the filter components of the converter is not taken into account for the subsequent analysis. Let the P and Q be the real power injected and reactive power drawn by IG. The line currents of the IG lags the respective phase voltage by θ_s which is given by (1)

$$\theta_s = 180^\circ - \tan^{-1}\left(\frac{Q}{P}\right)$$

$$\phi = tan^{-1}\left(\frac{Q}{P}\right) = 180^\circ - \theta_s \tag{1}$$

where $\phi \geq 0$.

To develop the phasor diagrams, the grid voltage at PCC, $\mathbf{V_{ab}}$ has been taken as the reference phasor

$$\mathbf{V_{ab}} = V\angle 0^\circ. \tag{2}$$

The magnitude of the grid and inverter voltages is V, which is the line to line voltage seen by the IG.

For the case where v_{cb} leads v_{ab}, the phase voltages and IG line currents are

$$\mathbf{V_{an}} = \frac{V}{\sqrt{3}}\angle -30^\circ, \quad \mathbf{I_{sa}} = I\angle -30^\circ + \phi$$

$$\mathbf{V_{bn}} = \frac{V}{\sqrt{3}}\angle -150^\circ, \quad \mathbf{I_{sb}} = I\angle -150^\circ + \phi$$

$$\mathbf{V_{cn}} = \frac{V}{\sqrt{3}}\angle 90^\circ, \quad \mathbf{I_{sc}} = I\angle 90^\circ + \phi. \tag{3}$$

The phase voltages and the IG line currents are shown in Fig. 4(b). The small italic fonts indicate instantaneous quantities of voltage and current, and capital bold fonts indicate the phasors. In this phasor diagram, the FEC current is relatively low owing to the fact that most of the real power injected by the IG is directly transferred to the grid.

B. Auxiliary Capacitor (C_{aux})

In this section reduction of APC current with the AC is presented. This work is based on the auxiliary capacitor assisted APC proposed in [17] for the induction motor load. The objective of this section is to validate the extension of the work presented in [15] to the IG and identify the appropriate location of the C_{aux} for ensuring the advantage of the converter pole currents reduction.

The IG line currents, with isolated neutral, are considered to follow relationship given in

$$i_{sa} + i_{sb} + i_{sc} = 0. \tag{4}$$

In addition to this, it is assumed that the fundamental component of the ripple filter capacitors is negligibly small as compared

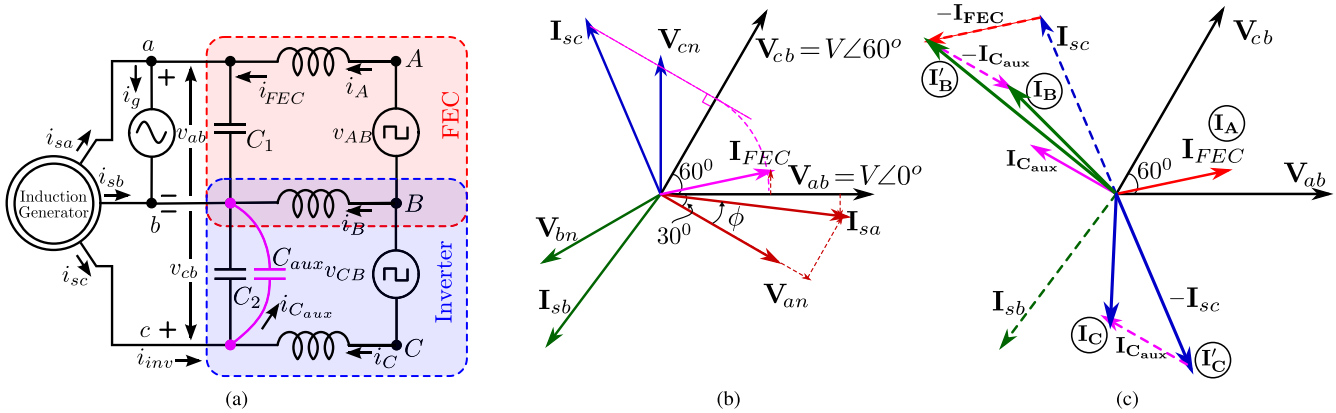

Fig. 4. Schematic and phasor diagram showing (a) AC based APC for IG with reduced converter currents, (b) IG current and voltage phasors, and (c) APC current phasors.

TABLE I
COMPARISON OF THE LINE VOLTAGE RELATION OF APC AND C_{AUX} LOCATION FOR OPTIMAL PERFORMANCE OF APC WITH IM AND IG

Machine	v_{cb}		C_{aux}	
	lags v_{ab}	leads v_{ab}	across a-c	across b-c
IM	✓	×	×	✓
IG	×	✓	×	✓

to the IG currents. The following relationship for the converter currents are obtained by applying Kirchhoff's current law (KCL) at nodes a, b, and c of Fig. 4(a) along with the above simplifying assumptions

$$\begin{aligned}\mathbf{I_A} &= \mathbf{I_{FEC}}\\ \mathbf{I_B} &= \mathbf{I_{sc}} - \mathbf{I_{FEC}} - \mathbf{I_{C_{aux}}}\\ \mathbf{I_C} &= -\mathbf{I_{sc}} + \mathbf{I_{C_{aux}}}\\ \mathbf{I_g} &= \mathbf{I_{sa}} + \mathbf{I_{FEC}}.\end{aligned} \tag{5}$$

From (5), it can be observed that the C_{aux} does not affect the converter Leg-A current, due to the current controlled FEC. The converter Leg-B and Leg-C currents, i_B, and i_C, respectively, changes with the $i_{C_{\text{aux}}}$. Using (5) and Fig. 4(b), the phasor diagram of APC pole currents shown in Fig. 4(c) can be drawn. Referring to Fig. 4(c), $\mathbf{I_B}'$ and $\mathbf{I_C}'$ are the APC leg-B and leg-C currents without C_{aux}. Inclusion of the C_{aux} modifies $\mathbf{I_B}'$ and $\mathbf{I_C}'$ to $\{\mathbf{I'_B} - \mathbf{I_{C_{aux}}}\}$ and $\{\mathbf{I'_C} + \mathbf{I_{C_{aux}}}\}$, respectively. The resultant AC-APC pole currents $\mathbf{I_B}$ and $\mathbf{I_C}$ have a reduced magnitude due to the AC, as indicated in Fig. 4(c). The phasor diagram qualitatively shows the effect of AC on reduction of the converter currents. Similarly, it can be shown that converter pole-B and pole-C currents increase with change the phase sequence or the location of AC across lines b and c to across lines a and b.

C. Comparison of APC With IM and IG

A comprehensive comparison with [8], [16]–[18] on application of APC with IM is provided in the Table I.

The desired APC phase sequence for IG and IM are opposite (conjugate of phasor voltages). However, the location of AC should be the same for both IM and IG.

IV. CONVERTER POLE CURRENTS

Analytical expressions to quantify the reduction in APC pole currents are derived in this section. Also, these expressions are used to obtain the optimum value for C_{aux}.

For an AC, C_{aux} with kVAR equals to $x\%$ of the IG kVA

$$x = V_{cb(\text{rms})} I_{C_{\text{aux}}(\text{rms})} / \sqrt{3} V I \Rightarrow I_{C_{\text{aux}}(\text{rms})} = x\sqrt{3} I \tag{6}$$

where V and I are the rms load voltage and current, respectively.

Referring to Fig. 4(b) where v_{cb} lags v_{ab}, the inverter voltage, current, and phase angle between them gives the real power demand, p_{INV}. The FEC draws real power p_{FEC} which equals to p_{INV} that is supplied to the inverter

$$p_{\text{FEC}} = p_{\text{INV}} \Rightarrow V \times Re\{I_{\text{FEC}}\} = VI\cos(30^\circ + \phi). \tag{7}$$

To operate APC with the grid current in phase with the grid voltage, the FEC supplies reactive component of the load phase-a current i_{sa}. The FEC current is

$$\mathbf{I_{FEC}} = I\cos(30^\circ + \phi) - jI\sin(30^\circ - \phi). \tag{8}$$

The APC leg-A rms current is given by

$$I_{A(\text{rms})} = |\mathbf{I_{FEC}}| = I\left[1 - 0.5\sqrt{3}\sin(2\phi)\right]^{1/2}. \tag{9}$$

The phase angle information of $\mathbf{I_{FEC}}$, $\mathbf{I_{C_{aux}}}$, and $\mathbf{I_{sc}}$ can be obtained from phasor diagram Fig. 4(b) and (c).

Using (5), the APC leg-B pole current $\mathbf{I_B}$ is given by

$$\begin{aligned}\mathbf{I_B} = {} & I\angle(90^\circ + \phi) - I\cos(30^\circ + \phi)\\ & + jI\sin(30^\circ - \phi) - x\sqrt{3}I\angle 150^\circ.\end{aligned} \tag{10}$$

The APC leg-B rms current can be simplified as follows

$$\begin{aligned}I_{B(\text{rms})} = {} & I\Big[1 + 0.5\sqrt{3}\sin(2\phi)\\ & + 3x^2 - 3x\sin(\phi) - 2\sqrt{3}x\cos(\phi)\Big]^{1/2}.\end{aligned} \tag{11}$$

Similarly, the AC-APC leg-C current can be expressed as

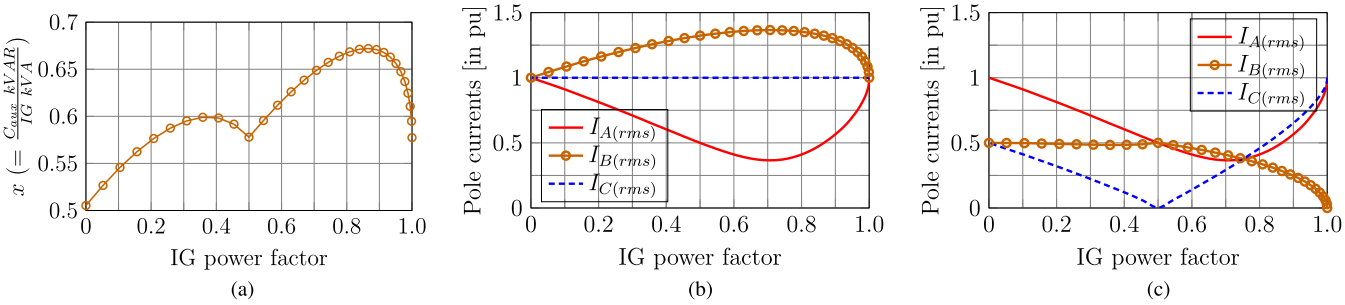

Fig. 5. Pole currents of the APC. (a) Optimal C_{aux} for different power factors of IG. (b) Converter currents without C_{aux}. (c) Converter currents with optimum C_{aux}.

$$\mathbf{I_C} = -I\angle(90^\circ+\phi) + x\sqrt{3}I\angle 150^\circ \tag{12}$$

$$I_{C(\text{rms})} = I\left[1+3x^2-3x\sin(\phi)-\sqrt{3}x\cos(\phi)\right]^{1/2}. \tag{13}$$

Referring to phasor diagram given in Fig. 4(b), current drawn from the grid $\mathbf{I_g}$ in (5) is obtained from the $\mathbf{I_{FEC}}$ and $\mathbf{I_{sa}}$.

The grid current is given in (14)

$$\begin{aligned}\mathbf{I_g} &= \mathbf{I_{FEC}}+\mathbf{I_{sa}}\\ &= I\cos(30^\circ+\phi)-jI\sin(30^\circ-\phi)+I\angle(30^\circ-\phi)\\ &= I\cos(30^\circ+\phi)+I\cos(30^\circ-\phi).\end{aligned} \tag{14}$$

The grid current in (14) can be simplified as

$$\mathbf{I_g} = \sqrt{3}I\cos(\phi) \quad \Rightarrow \quad I_{g(\text{rms})} = \sqrt{3}I|\cos(\phi)|. \tag{15}$$

The FEC current $\mathbf{I_{FEC}}$ and the load phase-a current $\mathbf{I_{sa}}$ and thus the grid current $\mathbf{I_g}$ are independent of the factor x which can be observed from (15).

A. Effect of Converter Power Loss and Ripple Filter Capacitor

The effect of inverter ripple filter capacitor, C_2, can be accounted by adding its value to C_{aux} which are both in parallel. On the other hand, the reactive current drawn by grid side ripple filter capacitor, C_1, offsets some part of the reactive poser drawn by IG. The power loss in the system would be taken from the IG and reflects as power loss in the converter and filter components. This results in a slight reduction of both real and imaginary parts of the expressions derived for $\mathbf{I_{FEC}}$ or $\mathbf{I_A}$ of the APC.

Moreover this power loss depends on converter and filter currents, device switching frequency. The reflection of $\mathbf{I_{FEC}}$ on the theoretically predicted grid current is small since, the power processed by the converter is small, thereby the $\mathbf{I_{FEC}}$ is also small fraction of $\mathbf{I_g}$.

B. Selection of Optimum C_{aux}

Analytical expressions of the APC pole currents reveal that the factor x (corresponding to the capacitance C_{aux}), load current (I) and power factor (ϕ) affect $I_{B(\text{rms})}$ and $I_{C(\text{rms})}$. Whereas, $I_{A(\text{rms})}$ is independent of the factor x. The value of C_{aux} can be chosen to minimize $I_{B(\text{rms})}$ or $I_{C(\text{rms})}$ or the converter volt-ampere (VA) S_{conv}, which is defined as

$$S_{\text{conv}} = V(I_{A(\text{rms})} + I_{B(\text{rms})} + I_{C(\text{rms})}). \tag{16}$$

Switching power loss and a part of conduction power loss in the IGBTs and diodes have a linear relationship with the absolute value of the device current. Typically, ohmic loss in semiconductor devices, which is a quadratic function of the device current, is a small fraction of the total semiconductor device power loss. The major part of the device power loss increases proportionally with the absolute value of the device current for state-of-the-art insulated-gate bipolar transistors (IGBTs). For an APC supplying 3.3 kVA inductive load at 25 kHz switching frequency, the device power loss proportional square of the rms current is close to 2.5% of the total device power loss that is proportional to the absolute value of the converter currents [17]. Hence, selecting the value of C_{aux} that minimizes S_{conv} in (16) is also a suitable choice for obtaining high efficiency. Since, C_{aux} has no effect on $I_{A(\text{rms})}$, a cost function $f_\sigma(\phi,x) \triangleq \{I_{B(\text{rms})}+I_{C(\text{rms})}\}$ is minimized and is sufficient for solving the optimization problem

$$x^* = \arg\min_x f_\sigma(\phi_o, x). \tag{17}$$

For a specific power factor ϕ_o, the optimum value of x that minimizes the cost function, $f_\sigma(\phi_o, x)$ is obtained numerically over a range of power factors $\phi_o \in [0, 90^\circ]$. The factor x that corresponds to the optimum C_{aux} using (17) is plotted in Fig. 5(a) for different power factors of the IG. The normalized pole currents with power factor from 0 to 1 without C_{aux} are given in Fig. 5(b). Whereas, Fig. 5(c) shows the reduced APC pole currents due to optimal C_{aux}.

V. Results and Discussion

The laboratory prototype consists of an IG mechanically coupled with an IM and variable frequency drive (VFD) as shown in Fig. 8. During start-up, the IG is driven above synchronous speed and the breaker of APC and IG is closed. Due to the small difference between the IG speed and its synchronous speed only minor transients are observed in the APC and IG line currents. The inrush currents in the case of IM starting from rest is about five times the rated current [8]. The power injected by the IG into the grid, can be controlled by the slip speed using the VFD driving the IG prime mover.

A challenging case study for the APC dynamic response is step change of reference voltage in the third phase while the converter is operating under no load, when damping is the least.

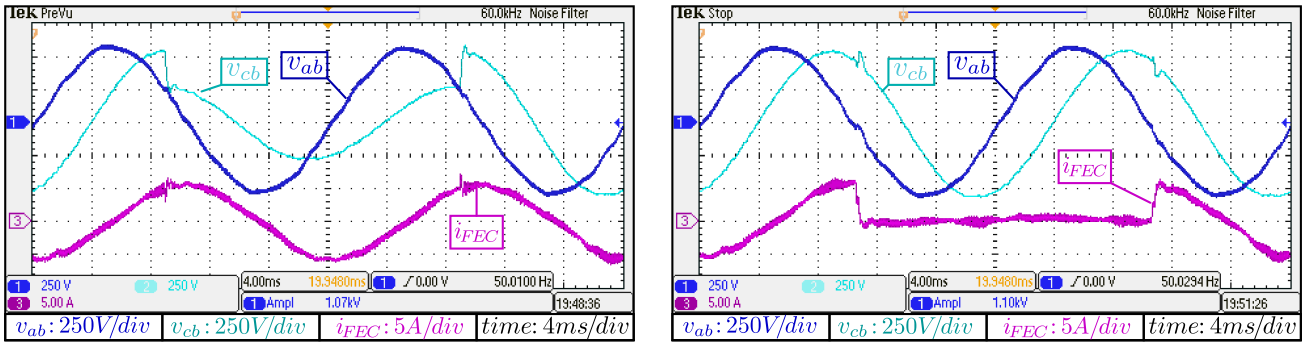

Fig. 6. Dynamic performance evaluation of the APC decoupled control. (a) Response of the FEC control to a step change in inverter voltage reference. (b) Response of the inverter control to a step change in FEC current reference.

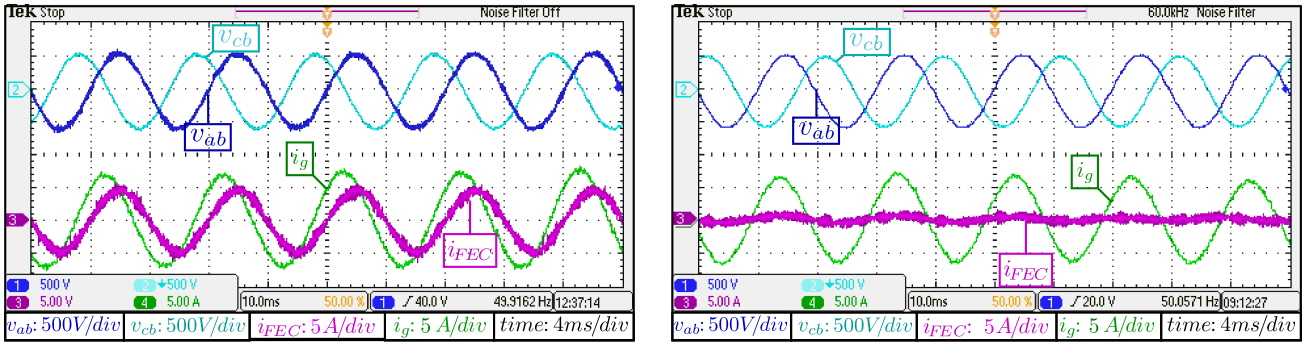

Fig. 7. Experimental results of the grid tied APC with no C_{aux} and powering a 3 kW IG rotating at 1560 r/min (1.04 p.u.) speed and injecting 1.5 kW power for lag and lead control methods. (a) v_{cb} lags v_{ab}. (b) v_{cb} leads v_{ab}.

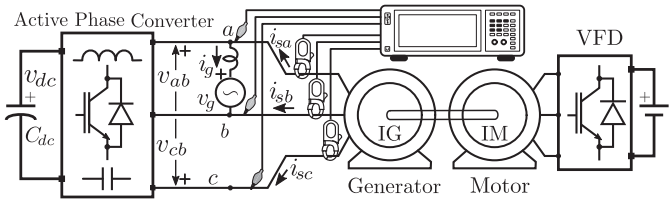

Fig. 8. Schematic of the experimental set-up for validation of the effect of C_{aux} on the APC pole currents.

The experimental results in Fig. 6(a) show the response of the inverter voltage controller for a step change in v_{cb} reference and FEC current controller action for a step change in inverter output voltage. The negligible disturbance in i_{FEC} during the step changes in v_{cb} demonstrates the validity of the decoupled control strategy. Fig. 6(b) shows the ability of the voltage controller to regulate the voltage v_{cb} for a step change in i_{FEC} as commanded. These results are for the case where v_{cb} lags v_{ab} and a reactive current command is given to the FEC in order to observe the disturbances in the i_{FEC}. A similar response is observed also with the complimentary case where v_{cb} leads v_{ab}. During dynamic study, it is observed the dynamic changes in mechanical torque on machine and sudden disconnection of the IG breaker have relatively less disturbance on the APC. This is due to the inertia of machine which lessens the impact of the load disturbance that is translated to the grid.

The experimental results of APC with IG is tested with two cases 1) v_{cb} lags v_{ab} 2) v_{cb} leads v_{ab} shown in Fig. 7 compare the effectiveness of appropriate reference voltage generation to reduce load on the converter and improve PF at the grid. Experimental results shown in Fig. 7(a) is for the cases where v_{cb} lags v_{ab} and Fig. 7(b) v_{cb} leads v_{ab}. In both the cases, IG is injecting 50% of rated power to the single-phase grid while running at 1560 r/min corresponding to a slip of -0.04 p.u. The effect of AC is studied for the case where v_{cb} leads v_{ab} which is preferred for the IG loads. The suitable C_{aux} varies from 28 to 50 μF for the IG used for experimental validation, where the maximum capacitance value is required at 80%–90% of full load. If the IG operates at a specific load for most of the time a fixed and optimal C_{aux} can be used. As a fixed C_{aux} is preferred in application, the average value of minimum and maximum optimal C_{aux}, 36 μF capacitor (including a 6 μF ripple filter capacitor, C_2) is used in the experimental validation. The APC generated line voltages applied across the IG terminals at full load are 395, 399, and 401 V. The deviation from the line voltages from the average value is $\pm 0.75\%$ showing a well balanced three-phase supply provided by the APC.

The application of APC for regeneration, using an IG is tested with two cases 1) without C_{aux} and 2) with a 30 μF C_{aux} in

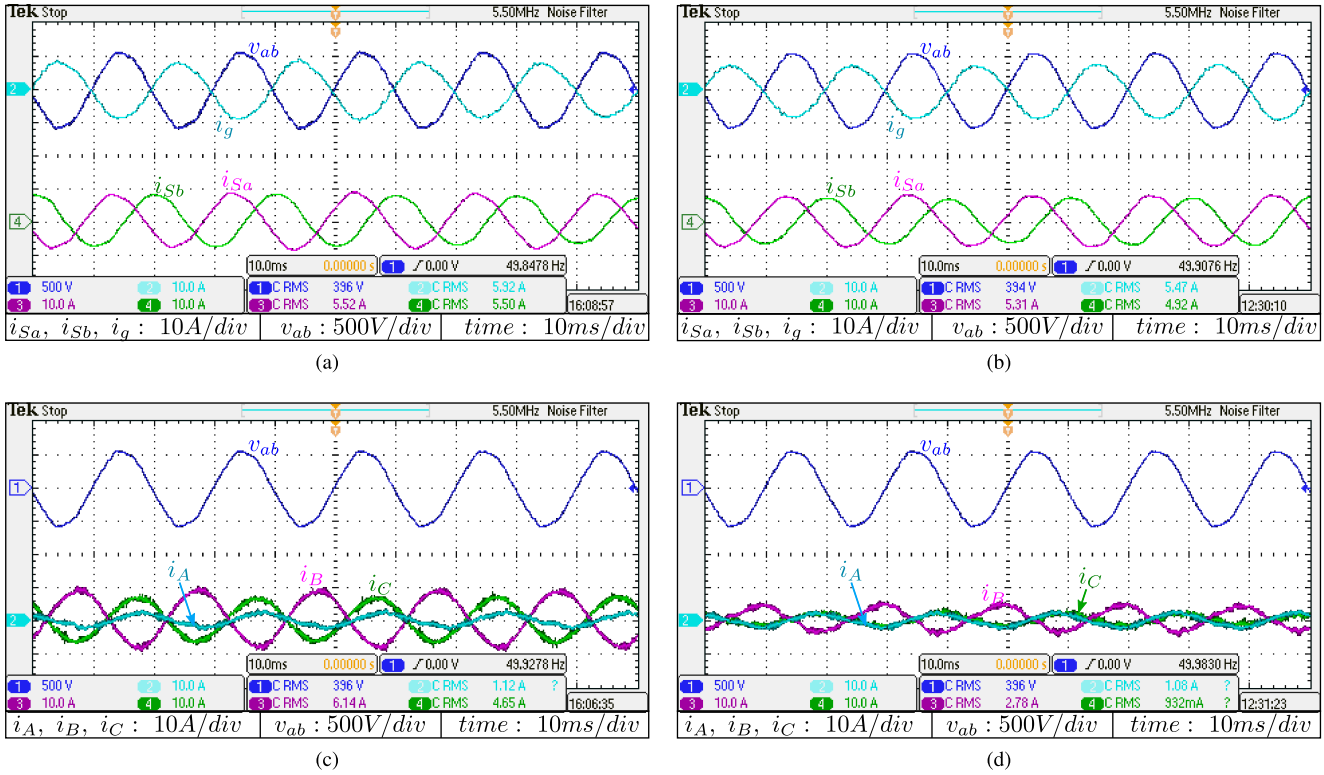

Fig. 9. Experimental results of the grid tied APC with the 3 kW IG rotating at 1580 r/min (1.05 p.u.) speed and injecting 2.4 kW power. (a) and (b) IG currents without and with 30 μF C_{aux}, respectively. (c) and (d) APC currents without and with 30 μF C_{aux}, respectively.

parallel with C_2, as discussed in Sections III and III-B. The experimental results shown in Fig. 9 compare the effectiveness of the AC C_{aux} for reduction of the APC pole currents. Experimental results shown in Fig. 9(a) and (b) show the IG operating condition in terms of the single-phase grid voltage, grid current, and IG line currents i_{sa} and i_{sb} for the cases with and without C_{aux}. The IG is injecting a 2.4 kW power 80% of rated power to the single-phase grid while running at 1580 r/min corresponding to a slip of -0.05 p.u. It can be observed that both the cases inject power to grid at close to UPF and IG line currents are indicating that the power delivered by the IG is almost the same. Fig. 9(c) shows the converter pole currents without C_{aux}. Inclusion of a 30 μF C_{aux} reduces the converter pole currents i_B and i_C as shown in Fig. 9(d). Whereas, the converter pole-A current i_A remains the same for both the cases as discussed in the analysis of Section III-B. The grid and converter rms currents and power injected to the grid recorded using the power analyser and oscilloscope are provided in Table II for a comparison with the theoretical values. The experimental findings closely match with the analysis. Ideally, total power delivered by the IG should be injected to the single-phase grid. But, the system power loss, depending on the converter operating conditions, reflects as a loss of power injected to the grid. The converter pole-A rms current has a small deviation from the theoretical values as expected due to the system power loss and ripple filter capacitor, C_1 as discussed in Section IV-A. The observed reduction in converter Leg-B and Leg-C rms currents is 55%

TABLE II
ANALYTICAL AND EXPERIMENTAL RESULTS OF GRID POWER WITH IG OPERATING INJECTING 2.4 KW LOAD

IG Operating Point	Parameter	$C_{aux}=0$		$C_{aux}=30\mu F$		Units
		Theor.	Exp.	Theor.	Exp.	
400V/5.4A 2.4 kW 3.7 kVA 0.64 PF 1580 RPM	$I_{g(rms)}$	6.01	5.85	6.01	5.81	A
	P_g	2.4	2.28	2.4	2.30	kW
	Q_g	0	0.28	0	0.27	kVAr
	Grid PF	1.0	0.99	1.0	0.99	–
	$I_{A(rms)}$	2.07	1.12	2.07	1.08	A
	$I_{B(rms)}$	6.63	6.14	3.27	2.78	A
	$I_{C(rms)}$	4.66	4.65	1.23	0.93	A

TABLE III
3 KW INDUCTION MACHINE PARAMETERS

Parameter	Value	Per unit
Rated voltage	415 V (Δ)	1.0
Stator resistance, R_s	1.56 Ω	0.047
Rated current	7.2 A	1.0
Stator leakage inductance, L_{ls}	18 mH	0.17
Rated power	3.0 kW	
Rotor resistance, R_r	2.62 Ω	0.079
Number of poles	4	
Rotor leakage inductance, L_{lr}	18 mH	0.17
Moment of inertia, J	0.1 kg-m^2	
Magnetizing inductance, L_o	177 mH	1.67

and 80%, respectively, showing less than 10% deviation from the pole current reduction expected from the theoretical expressions derived in this work.

VI. Conclusion

In this work, an AC based reduced switch APC in conjunction with an IG is proposed. The APC facilitates injection of power from a three-phase IG to a single-phase grid connection. From the qualitative analysis with the help of phasor diagrams, it is shown that the appropriate control and location of an auxiliary ac capacitor can reduce the APC pole currents significantly. A theoretical framework is presented to obtain the APC pole currents and grid current in the system. The experimental results are carried out on a 3 kW induction generator and using an APC prototype, with and without the AC. This work shows that the unique phase angle relationships that are required between the APC inverter voltage and single-phase grid voltage suitable for the IM and IG. However, the location for the AC can be the same for the APC with IM or IG. The results validate the effectiveness of the proposed method. The experimental results at 80% of the rated load of IG, the converter Leg-B, and Leg-C has shown a reduction of 55% and 80%, respectively.

Appendix

Induction motor parameters used for simulation and experimental studies are given in Table III.

References

[1] A. A. A. Aziz, R. A. Hamdy, A. S. Abdel-Khalik, and M. Y. A. Fattah, "Investigation of a three-phase self-excited induction generator feeding single-phase loads," in *Proc. 11th IEEE Int. Conf. Compat. Power Electron. Power Eng.*, Apr. 2017, pp. 358–363.

[2] E. C. dos Santos Jr., C. B. Jacobina, E. R. C. da Silva, and N. Rocha, "Single-phase to three-phase power converters: State of the art," *IEEE Trans. Power Electron.*, vol. 27, pp. 2437–2452, May 2012.

[3] O. Ojo, O. Omozusi, A. Ginart, and B. Gonoh, "The operation of a stand-alone, single-phase induction generator using a single-phase, pulse-width modulated inverter with a battery supply," *IEEE Trans. Energy Convers.*, vol. 14, no. 3, pp. 526–531, Sep. 1999.

[4] T. F. Chan and L. L. Lai, "Single-phase operation of a three-phase induction generator using a novel line current injection method," *IEEE Trans. Energy Convers.*, vol. 20, no. 2, pp. 308–315, Jun. 2005.

[5] J. B. Ekanayake, "Induction generators for small hydro schemes," *Power Eng. J.*, vol. 16, no. 2, pp. 61–67, Apr. 2002.

[6] Y. H. A. Rahim, A. I. Alolah, and R. I. Al-Mudaiheem, "Performance of single phase induction generators," *IEEE Trans. Energy Convers.*, vol. 8, pp. 389–395, Sep. 1993.

[7] T. F. Chan and L. L. Lai, "A novel excitation scheme for a stand-alone three-phase induction generator supplying single-phase loads," *IEEE Trans. Energy Convers.*, vol. 19, no. 1, pp. 136–143, Mar. 2004.

[8] A. K. Adapa and V. John, "Active-phase converter for operation of three-phase induction motors on single-phase grid," *IEEE Trans. Ind. Appl.*, vol. 53, no. 6, pp. 5668–5675, Nov. 2017.

[9] O. J. M. Smith, "Three-phase induction generator for single-phase line," *IEEE Power Eng. Rev.*, vol. 3, pp. 382–387, Sep. 1987.

[10] S. S. Murthy, C. S. Jha, and P. S. N. Rao, "Analysis of grid connected induction generators driven by hydro/wind turbines under realistic system constraints," *IEEE Trans. Energy Convers.*, vol. 5, no. 1, pp. 1–7, Mar. 1990.

[11] W. A. Oyekanmi, G. Radman, A. A. Babalola, and L. O. Uzoechi, "Effect of static VAR compensator positioning on a grid-connected wind turbine-driven squirrel cage induction generator," in *Proc. IEEE Int. Conf. Emerg. Sustain. Technol. Power ICT Developing Soc.*, Nov. 2013, pp. 247–252.

[12] S. Sugiarto, S. Islam, and A. Abu-Siada, "Power transfer capability improvement of an induction generator wind energy conversion system," in *Proc. TENCON 2009-2009 IEEE Region 10 Conf.*, Jan. 2009, pp. 1–6.

[13] O. Ojo, O. Omozusi, and A. A. Jimoh, "The operation of an inverter-assisted single-phase induction generator," *IEEE Trans. Ind. Electron.*, vol. 47, no. 3, pp. 632–640, Jun. 2000.

[14] M. Myers, M. Bodson, and F. Khan, "Design of drives for inverter-assisted induction generators," *IEEE Trans. Ind. Appl.*, vol. 48, no. 6, pp. 2147–2156, Nov. 2012.

[15] A. K. Adapa and V. John, "Reduced rating active phase converter for three phase induction generator based single phase grid-tied systems," in *Proc. IEEE Int. Conf. Power Electron. Drives Energy Syst.*, Dec. 2018, pp. 1–6.

[16] C. Chen, D. M. Divan, and D. W. Novotny, "A single phase to three phase power converter for motor drive applications," in *Proc. Conf. Record 1992 IEEE Ind. Appl. Soc. Ann. Meeting*, vol. 1, Oct. 1992, pp. 639–646.

[17] A. K. Adapa and V. John, "An auxiliary-capacitor-based active phase converter with reduced device current stress," *IEEE Trans. Ind. Electron.*, vol. 66, no. 9, pp. 6925–6935, Sep. 2019.

[18] A. Adapa, S. Bhowmick, and V. John, "Low-frequency DC-link capacitor current mitigation in reduced switch count single-phase to three-phase converter," *IEEE Trans. Ind. Electron.*, to be published.

[19] R. Teodorescu, F. Blaabjerg, M. Liserre, and P. C. Loh, "Proportional-resonant controllers and filters for grid-connected voltage-source converters," *IEE Proc. - Elect. Power Appl.*, vol. 153, no. 5, pp. 750–762, Sep. 2006.

[20] A. K. Adapa and V. John, "Virtual resistor based active damping of LC filter in standalone voltage source inverter," in *Proc. IEEE Appl. Power Electr. Conf. Expo.*, Mar. 2018, pp. 1834–1840.

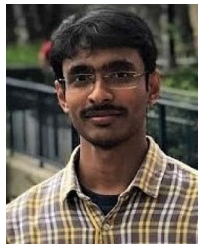

Anil K Adapa received the B.E. degree in electrical and electronics engineering from the Sagi Rama Krishnam Raju (SRKR) Engineering College, Bhimavaram, India, in 2009 and the M.E. and Ph.D. degrees in electrical engineering from the Department of Electrical Engineering, Indian Institute of Science, Bangalore, India, in 2011 and 2017, respectively.

He is currently working as a Research Associate with the Department of Electrical Engineering, Indian Institute of Science. He was with Medha Servo Drives Pvt. Ltd., Hyderabad, India, from 2011 to 2013, as Senior Engineer R&D. His research interests include power electronic converters hardware, power quality, digital control, and ac motor drives.

Vinod John (Senior Member, IEEE) received the B.Tech. degree from the Indian Institute of Technology, Madras, Chennai, India, in 1992, the M.S.E.E. degree from the University of Minnesota, Minneapolis, MN, USA, in 1994, and the Ph.D. degree from the University of Wisconsin, Madison, WI, USA, in 1999, all in electrical engineering.

He is currently an Associate Professor with the Department of Electrical Engineering, Indian Institute of Science, Bangalore, India. His research interests include switched mode power conversion, power quality, and distributed generation.